Original Article

CENPA-driven STMN1 Transcription Inhibits Ferroptosis in Hepatocellular Carcinoma

Daomiao Liang[1], Lanzhu Luo[2], Jiang Wang[2], Tongyu Liu[1] and Chao Guo[1*]

[1]Department of Hepatobiliary Surgery, The First Affiliated Hospital of Hunan Normal University (Hunan Provincial People's Hospital), Changsha, Hunan, China; [2]Children's Medical Center, The First Affiliated Hospital of Hunan Normal University (Hunan Provincial People's Hospital), Changsha, Hunan China

Abstract

Background and Aims: The growing knowledge of ferroptosis has suggested the regulatory role of ferroptosis in hepatocellular carcinoma (HCC), but the pertinent molecular mechanisms remain unclear. Herein, this study investigated the mechanistic basis of ferroptosis-related genes (ferrGenes) in the growth of HCC. ***Methods:*** Differentially expressed human ferrGenes and tumor-related transcription factors (TFs) were obtained from the The Cancer Genome Atlas (TCGA) dataset and the GTEx dataset. Spearman method-based correlation analysis were conducted to construct TF-ferrGene coexpression regulatory network. Key genes associated with prognosis were singled out with Lasso regression and multivariate Cox analysis to construct the prognostic risk model. Then the accuracy and independent prognostic ability of the model were evaluated. Expression of CENPA and STMN1 was determined in clinical HCC tissues and HCC cells, and their binding was analyzed with dual-luciferase and chromatin immunoprecipitation (ChIP) assays. Furthermore, ectopic expression and knockdown assays were performed in HCC cells to assess the effect of CENPA and STMN1 on ferroptosis and malignant phenotypes. ***Results:*** The prognostic risk model constructed based on the eight TF-ferrGene regulatory network-related genes accurately predicted the prognosis of HCC patients. It was strongly related to the clinical characteristics of HCC patients. Moreover, CENPA/STMN1 might be a key TF-ferrGene regulatory network in ferroptosis of HCC. CENPA and STMN1 were overexpressed in HCC tissues and cells. Additionally, CENPA facilitated STMN1 transcription by binding to STMN1 promoter, thus facilitating the malignant phenotypes and suppressing the ferroptosis of HCC cells. ***Conclusions:*** Taken together, CENPA curbs the ferroptosis of HCC cells by upregulating STMN1 transcription, thereby promoting HCC growth.

Citation of this article: Liang D, Luo L, Wang J, Liu T, Guo C. CENPA-driven STMN1 Transcription Inhibits Ferroptosis in Hepatocellular Carcinoma. J Clin Transl Hepatol 2023;11(5): 1118–1129. doi: 10.14218/JCTH.2023.00034.

Introduction

Hepatocellular carcinoma (HCC) is among the most frequent neoplasm worldwide, with increasing incidence.[1,2] Moreover, treatment responses vary in HCC patients with similar disease phenotypes because of different molecular etiologies, so stratifying patients at the molecular level can contribute to the development of the most effective treatment regimen.[3] As a result, it is warranted to further the research of molecular mechanisms underlying HCC.

Ferroptosis, iron-dependent regulated cell death, is featured by redox imbalance and intracellular lipid peroxide accumulation and demonstrates distinguishable biological and morphological features from other cell death patterns.[4] Ferroptosis refers to the result of membrane lipid peroxidation (LPO) caused by loss or insufficiency of the selenoperoxidase glutathione peroxidase 4 (GPX4).[5] Ferroptosis has been extensively accepted as a pivotal anti-oncogenic mechanism, and impeded ferroptosis has been confirmed to contribute to tumor development.[6] Since the liver is a critical site of iron metabolism, ferroptosis exhibits an essential effect in the carcinogenesis of HCC and, moreover, may have the potential to eradicate HCC.[7] Furthermore, Liang *et al*.[8] established a novel ferroptosis-related gene (ferrGene) signature for the prognostic prediction of HCC, suggesting targeting ferroptosis as a promising therapeutic alternative for HCC. In addition, another research revealed that elevated ferroptosis by COMMD10 facilitated radiosensitivity of HCC cells.[9] Therefore, an in-depth understanding of ferrGenes in HCC

may have important implications for the treatment of HCC.

Transcription factors (TFs) mediate multiple normal cell processes, like cell proliferation, immune responses, metabolism, differentiation, and apoptosis.[10] TFs are a distinct group of drug targets that orchestrate aberrant gene expression, such as blockade of differentiation and cell death gene expression, and are altered in numerous cancers.[11] Importantly, multiple TFs have been implicated in the onset and progression of HCC. For instance, AP-4 facilitates tumorigenesis in HCC.[12] Likewise, c-Myb fosters the invasion of HCC cells.[13] Moreover, TFs can bind to DNA response elements to modulate gene expression.[14] Meanwhile, TFs have been reported to regulate ferrGenes to control ferroptosis. For example, the TF BACH1 facilitates ferroptosis by depressing the transcription of a subset of erastin-induced protective genes that participate in glutathione (GSH) synthesis or intracellular labile iron metabolism, including Gclm, Slc7a11, Fth1, Ftl1, and Slc40a1.[15] Therefore, the identification of TF-ferrGene regulatory networks increases our understanding of the pathogenesis of HCC and the development of novel treatments. In this context, we identified TF-ferrGene regulatory networks and constructed a prognostic risk model associated with the networks with bioinformatics analysis, and confirmed the predicted results in cell culture experiments.

Methods

Ethics statement

The study was approved by the Ethics Committee of our Hospital and conducted in strict accordance with the Declaration of Helsinki. All participants signed informed consent documentation before sample collection.

Clinical sample collection

This study enrolled 32 patients 31 to 68 years of age who were diagnosed with liver cancer by needle aspiration biopsy and pathological diagnosis at Hepatobiliary Surgery of our Hospital from September 2017 to February 2019. The inclusion criteria were based on the standards of the World Health Organization.[16] Tissue samples were confirmed confirmed to contain more than 80% tumor cells by pathological examination, and adjacent normal tissues were at least 5 cm from the tumor edge. Patients had not received anticancer treatment prior to surgery. Tumor nodules were completely resected, as confirmed pathologically by the absence of tumor tissue on the resected surface. Patients had complete clinicopathological and follow-up data. Patients who died from non-HCC diseases or accidents were excluded.

Microarray data downloading

The HCC expression data in The Cancer Genome Atlas (TCGA) and Genotype-Tissue Expression (GTEx) project were downloaded from the UCSC Xena database. Meanwhile, the phenotypic and clinical prognosis data of HCC tissue samples were downloaded from TCGA. The TCGA dataset included 50 normal liver tissue samples, 374 HCC tissue samples, and the clinical data of 365 HCC patients, and the GTEx dataset included 110 normal liver tissue samples. The type of all data types was Fragment Per Kilobase Million. Microarray annotation information was obtained from the Gencode database. The ID of TCGA and GTEx datasets was transformed with the Perl language. Data in the two datasets were merged, retaining only the genes annotated in both TCGA and GTEx datasets, after which 160 normal liver tissue samples and 374 HCC tissue samples were attained.

Differentially expressed gene (DEG) analysis

Data in TCGA and GTEx datasets were merged. Human ferrGene information was obtained with the online website (http://www.zhounan.org/), and human tumor-related TF information was collected with the online website (http://cistrome.org/). Subsequently, ferrGenes and tumor-associated TFs were extracted from the merged data and subjected to DEG analysis using the R language limma package with normal liver tissue samples as the control. The differential p-values were corrected with the false discovery rate (FDR) method, and |log (fold change)|>1 and FDR<0.05 was the screening threshold for significantly differentially expressed ferrGenes and tumor-related TFs.

TF-ferrGene coexpression regulatory network

Differentially expressed TFs and ferrGenes were subjected to correlation analysis using the Spearman method, with the correlation coefficient cor>0.4 and the relevance $p<0.05$ as the screening criteria. The negative correlation between a TF and a ferrGene suggested that this TF negatively regulates the ferrGene, and vice versa, its positively regulates the ferrGene. The TF-ferrGene coexpression regulation network was constructed based on the results of the TF-ferrGene correlation analysis with the cytoscape v3.7.1 software.

Prognostic risk model construction

The prognostic risk model was constructed after the Lasso regression and multivariate Cox analysis of genes in the TF-ferrGene regulatory network with the survival package and the calculation of risk values for each HCC patient. The R language survival and survminer packages were used to plot survival curves based on the prognostic risk model, followed by the calculation of p-values. Patients were classified into high-risk and low-risk groups based on the median value of the risk score. Kaplan-Meier survival analysis were performed to compare the overall survival (OS) between the high-risk and low-risk groups, with $p<0.05$ as the cutoff value. The prognostic risk model was subjected to receiver operating characteristic (ROC) curve analysis with the survivalROC package, and then the Area Under the ROC Curve (AUC) value was calculated. The gene nomogram of the genes involved in the construction of the prognostic risk model was drawn with the rms package, and the calibration curve was plotted to assess the consistency between the actual and predicted values. Multivariate Cox regression analysis was used to analyze the independent prognostic power of the prognostic risk model.

Clinical correlation analysis

The expression and high- and low-risk distribution of the genes involved in the construction of the prognostic risk model were integrated with clinical traits. Thereafter, the clinical analysis of these genes was conducted with the R language limma and pheatmap packages, followed by the delineation of a heatmap.

Lentiviral vector construction

The lentiviral overexpression vector pCDH-CMV-MCS-EF1-copGFP (CD511B-1; System Biosciences, Palo Alto, CA, USA) and the lentiviral silencing vector pSIH1-H1-copGFP (SI501A-1; System Biosciences) were purchased for constructing the overexpression vectors of CENPA and STMN1 and the silencing vectors of CENPA, as well as their negative control (NC). The lentivirus particles were packaged into HEK-293T cells (iCell-h237; iCell Bioscience, Shanghai, China) with Lentivirus Packaging Kits (A35684CN; Invitrogen, Carlsbad, CA, USA), and the cell supernatant was collected

after 48 h as lentivirus with a titer of 1×10^8 TU/mL. The used shRNA sequences were as follows: short hairpin (sh)-NC, CTATGCCGATAAGTCATTAGC; sh-CENPA-1, GCCTATCTC-CTCACCTTACAT; sh-CENPA-2, CCGAGTTACTCTCTTCCCAAA (Supplementary Table 1).

Cell culture and transduction

Normal hepatocytes (THLE-2; MZ-4049) and HCC cell lines Huh-7 (MZ-0095), JHH7 (MZ-2707), and SNU387 (MZ-2671) were purchased from Ningbo Mingzhou Biotechnology Co., Ltd. (Ningbo, China). THLE-2 cells were cultured in 1,640 medium containing 10% fetal bovine serum (FBS; Sigma-Aldrich, St Louis, MO, USA), and Huh-7, JHH7, and SNU387 were cultured in Dulbecco's Modified Eagle Medium with 10% FBS and 1% penicillin/streptomycin (MCM-0120; Ningbo Mingzhou Biotechnology Co., Ltd.). Huh-7 cells were arranged into overexpression (oe)-NC, oe-CENPA, sh-NC, sh-CENPA, sh-NC + oe-NC, sh-CENPA + oe-NC, and sh-CENPA + oe-STMN1 groups. Specifically, 1 mL corresponding lentivirus was added to Huh-7 cells, and the lentiviral infection effect was detected subsequent to 48 h.

Western blot analysis

The cell or tumor tissue precipitate was lysed in lysis buffer. The homogenates were put on ice for 10 m and centrifuged (3,000 *g*, 4°C, 10 m). The supernatant was transferred to a precooled Eppendorf tube. Following protein concentration determination by BCA kits, the proteins were transferred to a PVDF membrane and blocked with 5% BSA at room temperature for 1 h and incubated with antibodies against CENPA (ab45694, 1:1,000; Abcam, Cambridge, UK), STMN1 (ab52630, 1:10,000; Abcam), and ACTIN (ab8226, 1:1,000; Abcam) overnight at 4°C. The next day, the proteins were incubated with the secondary antibody at room temperature for 1 h, followed by development on the gel imaging system. The protein bands were subjected to grayscale scanning with AlphaView SA software (Version: 3.4.0).

Immunofluorescence

A total of 1×10^5 HCC cells were seeded on a coverslip and cultured for 24 h. After being fixed with 4% formaldehyde for 20 m, the cells were permeated with 0.5% Triton X-100 in phosphate buffer saline (PBS) for 10 m at room temperature. After 10 m of blockade with 2% BSA in PBS-0.1% Triton X-100, the cells were incubated with alpha-fetoprotein (AFP) antibody (ab284388, 1:100; Abcam) overnight at 4°C. The cells were then incubated with fluorescence-labeled secondary antibody and 4',6-diamidino-2-phenylindole (DAPI) at room temperature for 2 h, followed by recording of cell images under a confocal microscope.

Reverse transcription-quantitative polymerase chain reaction (RT-qPCR)

Total RNA of cells was extracted with TRIzol (Thermo Fisher Scientific, Waltham, MA, USA), followed by measurement of RNA concentration and purity with a NanoDrop2000 trace ultraviolet spectrophotometer (Thermo Fisher Scientific). The obtained RNA was reversely transcribed to generate cDNA as instructed in the manuals of the PrimeScript RT reagent kit (RR047A; TaKaRa, Tokyo, Japan). CENPA and STMN1 primers were synthesized by TaKaRa (Supplementary Table 2). qRT-PCR was performed on a 7500 Fast real-time PCR system (4351106; Thermo Fisher Scientific). With glyceraldehyde 3-phosphate dehydrogenase (GAPDH) as the housekeeping gene, the relative transcription level of target genes was calculated with the $2^{-\Delta\Delta CT}$ method.

Dual-luciferase assay

oe-NC, oe-CENPA, sh-NC, and sh-CENPA were co-transfected with a luciferase reporter plasmid containing the STMN1 promoter sequence (CTCGTATAGCAAA) into human embryonic kidney HEK293T cells using the lipofectamine 2000 kit (11668019; Thermo Fisher Scientific) for assessing the effect of CENPA on the transcription activity of STMN1 promoter. Cells were lysed 48 h subsequent to transfection, and luciferase activity was measured with a luciferase assay kit (K801-200; BioVision, San Francisco, CA, USA) on a dual-luciferase reporter assay system (Promega, Madison, WI, USA). With Renilla luciferase employed as an internal reference, the activation degree of the target reporter gene was compared according to the ratio of relative luciferase units between firefly luciferase activity and Renilla luciferase activity.

ChIP assay

The enrichment of CENPA in STMN1 promoter was detected with a ChIP kit (KT101-02, Saicheng Biotechnology Co., Ltd., Guangzhou, China). In detail, upon cell confluence of 70–80%, cells were fixed with 1% formaldehyde at room temperature for 10 m to crosslink intracellular DNA and protein. After cross-linking, DNA was randomly broken by ultrasonic treatment to fragments of appropriate size with 10 s each time at the interval of 10 s for 15 cycles. After cell centrifugation at 13,000 rpm at 4°C, the supernatant was collected and divided into three tubes which were respectively supplemented with RNA polymerase II rabbit antibodies (positive control; 1:100, ab238146; Abcam), rabbit anti-immunoglobulin G antibodies (NC; ab172730, 1:100; Abcam) and the target protein-specific antibody, rabbit anti-CENPA (1:50, H00001059-PW1; Novus Biological, Littleton, CO, USA) for overnight incubation at 4°C. Endogenous DNA-protein complexes were precipitated with Protein Agarose/Sepharose and transiently centrifuged, followed by the removal of the supernatant. The nonspecific complexes were washed before overnight uncross-linking at 65°C. Phenol/chloroform extraction was utilized to purify and recover DNA fragments for the qPCR detection of the promoter fragment of STMN1. Primers specific for STMN1 promoter were as follows: forward, CTTGGGCACCCCTTAGTTGT and reverse, AATTGGTCTGACCG TGCCTT.

Enzyme-linked immunosorbent assay (ELISA)

Cell lysates were tested strictly as per the protocols of ELISA kits (glutathione [GSH]: JN20809, Jining Industrial Co., Ltd, Shanghai, China; glutathione peroxidase 4 [GPX4]: JL46163, Shanghai Jianglai Industrial Co., Ltd., Shanghai, China; reactive oxygen species [ROS]: JL13783, Shanghai Jianglai Industrial Co., Ltd., and malondialdehyde [MDA]: JL11466, Shanghai Jianglai Industrial Co., Ltd.) to detect the levels of GSH, GPX4, MDA, and ROS.

Fe^{2+} detection

The enrichment of Fe^{2+} was detected with an iron content detection kit (MAK025-1KT; Sigma-Aldrich). Specifically, cells were detached with 0.25% trypsin, centrifuged, and precipitated, followed by centrifugation with 4 times the volume of iron assay buffer in a cold centrifuge and the collection of the supernatants. Afterwards, 50 μL supernatants were added to 96-well plates, and then 5 μL Fe^{2+} analysis buffer was added to each sample well and Fe^{2+} standard sample well, followed by 30 m of incubation at room temperature. Fe^{2+} probe reagents (100 μL) were added to each sample well and Fe^{2+} standard sample well and incubated for 60 m at room
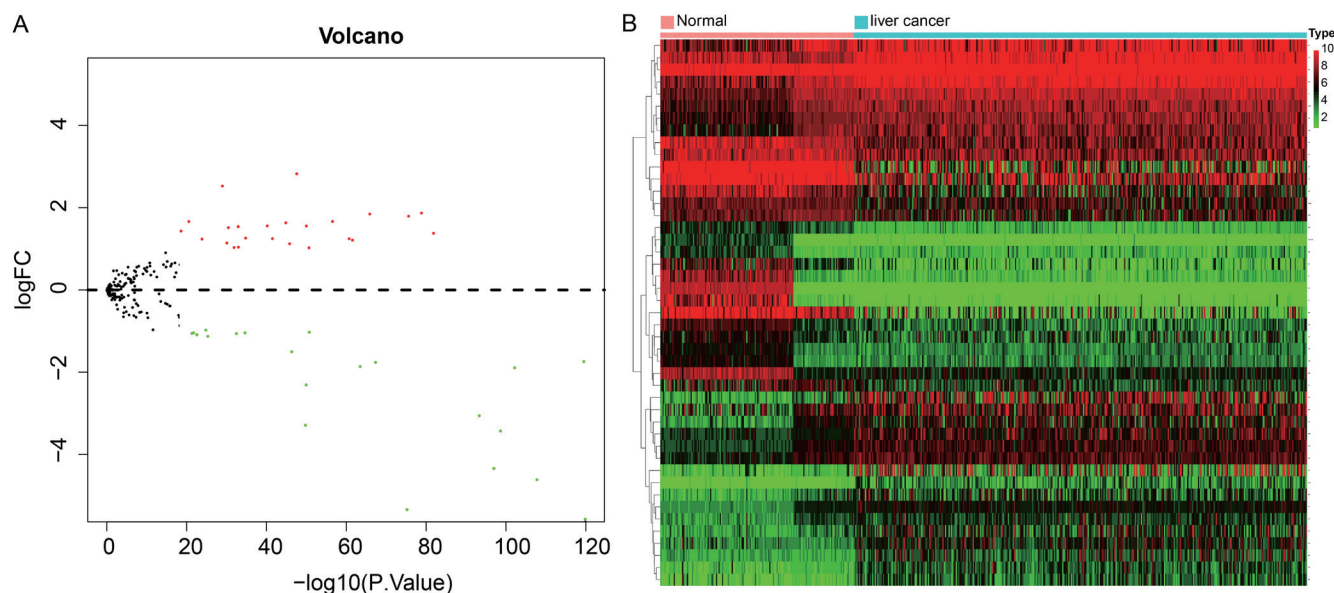
Fig. 1. Differentially expressed ferrGenes in HCC. (A) Volcano map of differentially expressed ferrGenes in datasets. Black dots represent genes that are not differentially expressed, red dots represent the upregulated ferrGenes, and green dots indicate downregulated ferrGenes. (B) Heatmap of differentially expressed ferrGenes in the HCC-related TCGA dataset combined with the GTEx dataset. The left dendrogram indicates gene clustering based on gene expression, and the top right histogram shows the color scale. Red indicates highly expressed genes, green represents poorly expressed genes, blue indicates HCC tissue samples (374 cases), and pink indicates normal liver tissue samples (160 cases). ferrGene, ferroptosis-related gene; GTEx, Genotype-Tissue Expression; HCC, hepatocellular carcinoma; TCGA, The Cancer Genome Atlas.

temperature in darkness for the full loading of probes. For Fe^{2+} analysis, 50 μL samples were added to the sample wells of the 96-well plates, and 5 μL analysis buffer was added to each sample well for 30-min incubation of iron standards and samples to be tested at 25°C. After that, 100 μL Fe^{2+} probes were added to each well containing the iron standards and tested samples and mixed evenly, followed by 60 m of reaction at 25°C in darkness. Optical density (OD) values at 593 nm were measured with a microplate reader.

Flow cytometry

Cell apoptosis was detected with an annexin V-fluorescein isothiocyanate (FITC)/propidium iodide (PI) double staining. In detail, the treated cells were placed in a 37°C incubator containing 5% CO_2 for 48 h culture. Next, cells were washed twice with PBS, centrifuged, and resuspended in 200 μL binding buffer. Cells were supplemented with 10 μL annexin V-FITC (ab14085; Abcam) and 5 μL PI and gently mixed. Thereafter, cells were reacted with 300 μL binding buffer for 15 m in the dark. Finally, apoptosis was assayed by flow cytometry with an excitation wavelength of 488 nm.

Cell counting kit (CCK)-8

Cell viability was examined with a CCK-8 kit (CA1210; Solarbio, Beijing, China). Briefly, logarithmically growing cells were seeded into the 96-well plates at 1×10^4 cells per well for 24 h of preculture, followed by transfection. Subsequently, 10 μL CCK-8 reagents were added at 0, 24, 48, and 72 h after transfection and cultured at 37°C for 3 h. OD values were measured with a microplate reader at 450 nm.

Statistical analysis

Statistical analysis of the data was performed with SPSS software (version 21.0; IBM Corp., Armonk, NY, USA). Measurement data were reported as means ± standard deviation.

Normally distributed data were compared with the unpaired Student's *t*-test between two groups and with one-way analysis of variance among multiple groups, with Tukey's for *post hoc* tests. A *p*-value<0.05 was considered a statistically significant difference.

Results

Differentially expressed ferrGenes in HCC

We screened out ferrGenes in HCC with bioinformatics analysis. Specifically, HCC-related expression data were obtained from TCGA through the UCSC Xena database, including 50 normal liver tissue samples and 374 HCC tissue samples. To further expand the sample size and increase the number of normal liver tissue samples, we obtained 110 normal liver tissue samples from the GTEx database. The data of TCGA and GTEx datasets were merged and corrected. Afterwards, human ferrGene information was harvested with the online website (http://www.zhounan.org/). FerrGenes were extracted from the merged data and subjected to differential analysis, yielding 45 significantly differentially expressed ferrGenes including 24 upregulated ferrGenes and 21 downregulated ferrGenes (Fig. 1A, B). In conclusion, 45 differentially expressed ferrGenes in HCC were successfully screened with TCGA combined with the GTEx dataset.

Differentially expressed TFs co-expressed with ferrGenes in HCC

To screen TFs co-expressed with ferrGenes, the human tumor-related TF information was attained through an online website (http://cistrome.org/), and tumor-related TFs were extracted from the datasets for differential analysis. A total of 32 significantly differentially expressed TFs were obtained in HCC patients (Fig. 2A). Next, the coexpression analysis of these 32 TFs and 45 differentially expressed ferrGenes
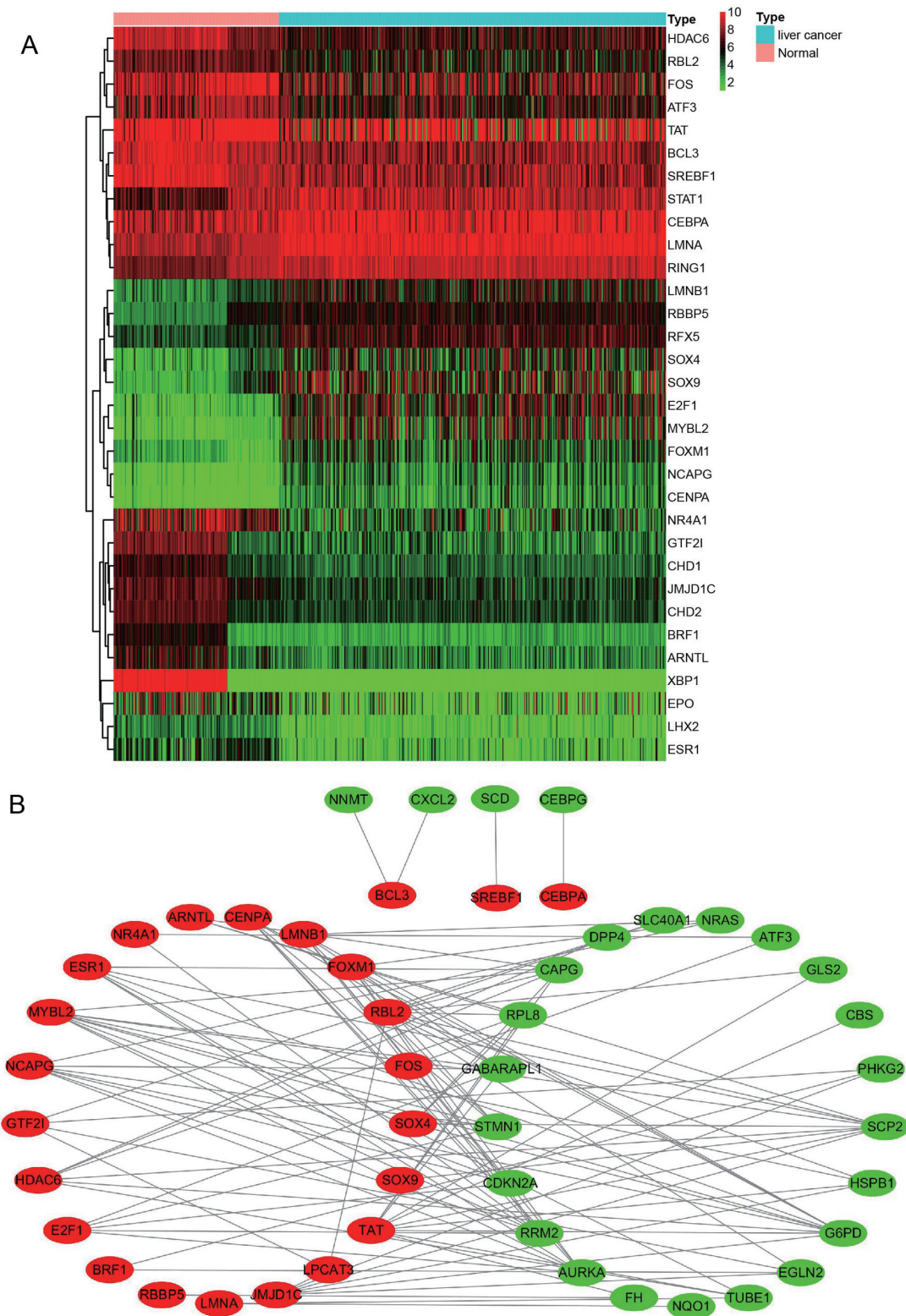
Fig. 2. Differential analysis of TFs and construction of the TF-ferrGene regulatory network. (A) Heatmap of differentially expressed TFs from the HCC-related TCGA dataset combined with the GTEx dataset. The left dendrogram indicates gene clustering based on gene expression, and the top right histogram indicates the color scale. Red indicates highly expressed genes, green indicates lowly expressed genes, blue indicates HCC tissue samples (374 cases), and pink indicates normal liver tissue samples (160 cases). (B) Visualization of the TF-ferrGene regulatory network with Cytoscape. Red represents TFs, and green represents ferrGenes. HCC, hepatocellular carcinoma; TF, transcription factor; ferrGene, ferroptosis-related gene; GTEx, Genotype-Tissue Expression; TCGA, The Cancer Genome Atlas.
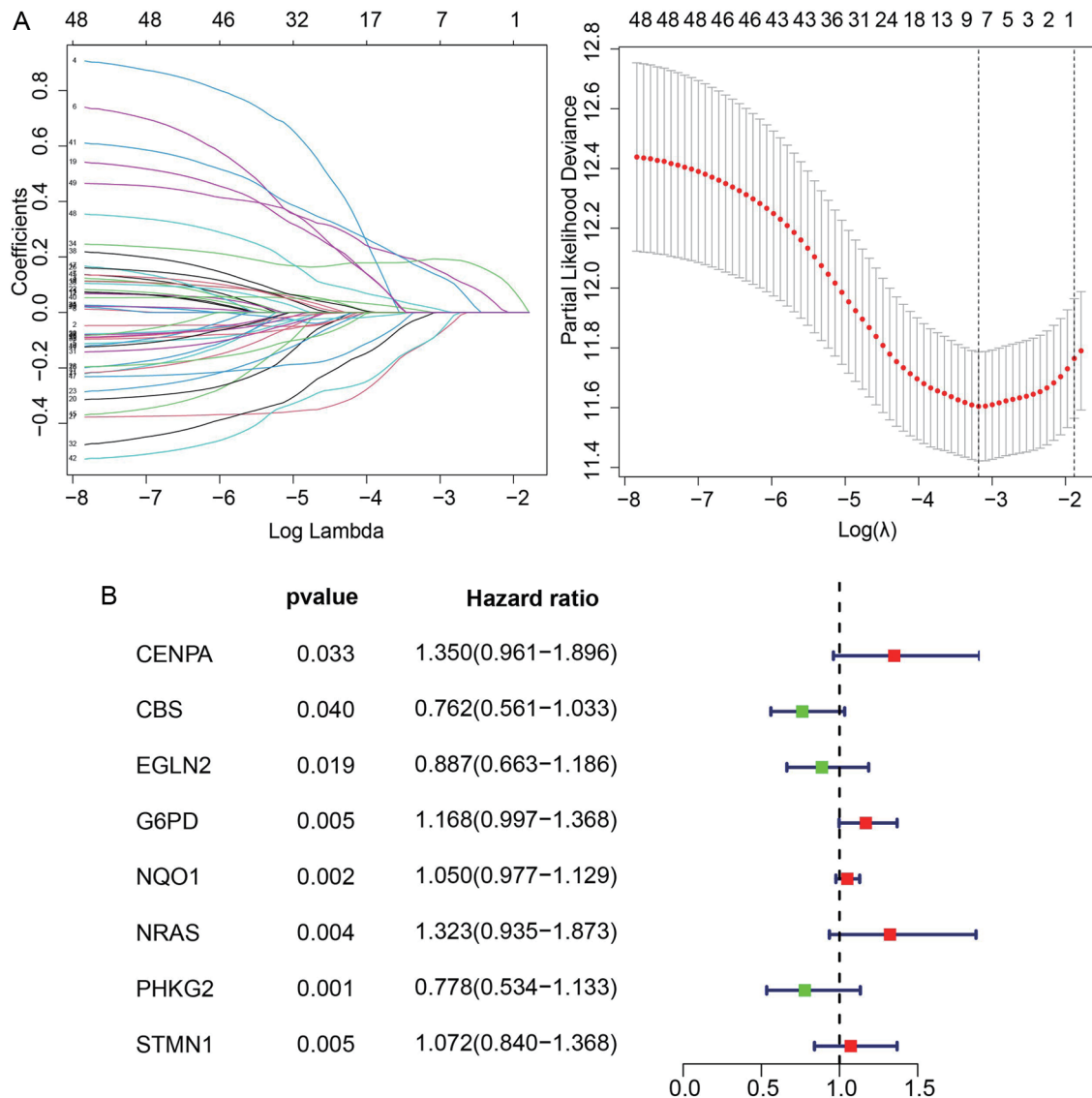
Fig. 3. Construction of a prognostic risk model for HCC patients. (A) Lasso coefficient distribution of 49 genes in HCC. (B) Selection of the optimal parameter (lambda) in the Lasso analysis of HCC. (C) The forest map of the multivariate Cox analysis. Left side shows the name of DEGs, and the middle shows the *p*-value. The hazard ratio (HR) represents risk. An HR>1 indicates a high-risk gene an HR<1 indicates a low-risk gene. The right side shows the HR distribution of the gene, where distribution on the left side indicates low risk and distribution on the right side represents high risk. DEG, differentially expressed gene; HCC, hepatocellular carcinoma.

revealed that 23 TFs were co-expressed with 26 ferrGenes (Fig. 2B). The above data illustrated that the TF-ferrGene regulatory network might play an essential part in HCC progression.

TF-ferrGene regulatory network-related genes are closely related to the prognosis of HCC patients

The investigation further moved to assess the relationship between the related genes in the TF-ferrGene regulatory network and the prognosis of HCC patients. We integrated the clinical survival data of HCC patients in the TCGA dataset with the expression data of the related genes in the TF-ferrGene regulatory network. Thereafter, eight genes were obtained with Lasso regression and multivariate Cox analysis (Fig. 3A–C). Among them, CENPA, G6PD, NQO1, NRAS, and STMN1 were high-risk genes, which indicated that their high

expression was associated with poor prognosis. Whereas, CBS, EGLN2, and PHKG2 were low-risk genes, which indicated that their low expression was associated with poor prognosis. In summary, a prognostic risk model of HCC patients was constructed based on the expression of eight genes.

A prognostic risk model based on the eight genes accurately predicts prognosis of HCC patients

The risk value for each sample was calculated with the prognostic risk model. With the median risk value as the distinguishing boundary, the HCC patients in the TCGA dataset were assigned to high-risk (182 patients) and low-risk (183 patients) groups (Fig. 4A). Statistical analysis of the clinical survival data of HCC patients in the high-risk and low-risk groups (Fig. 4B) found that deaths in the high-risk group were significantly increased relative to those in the low-risk
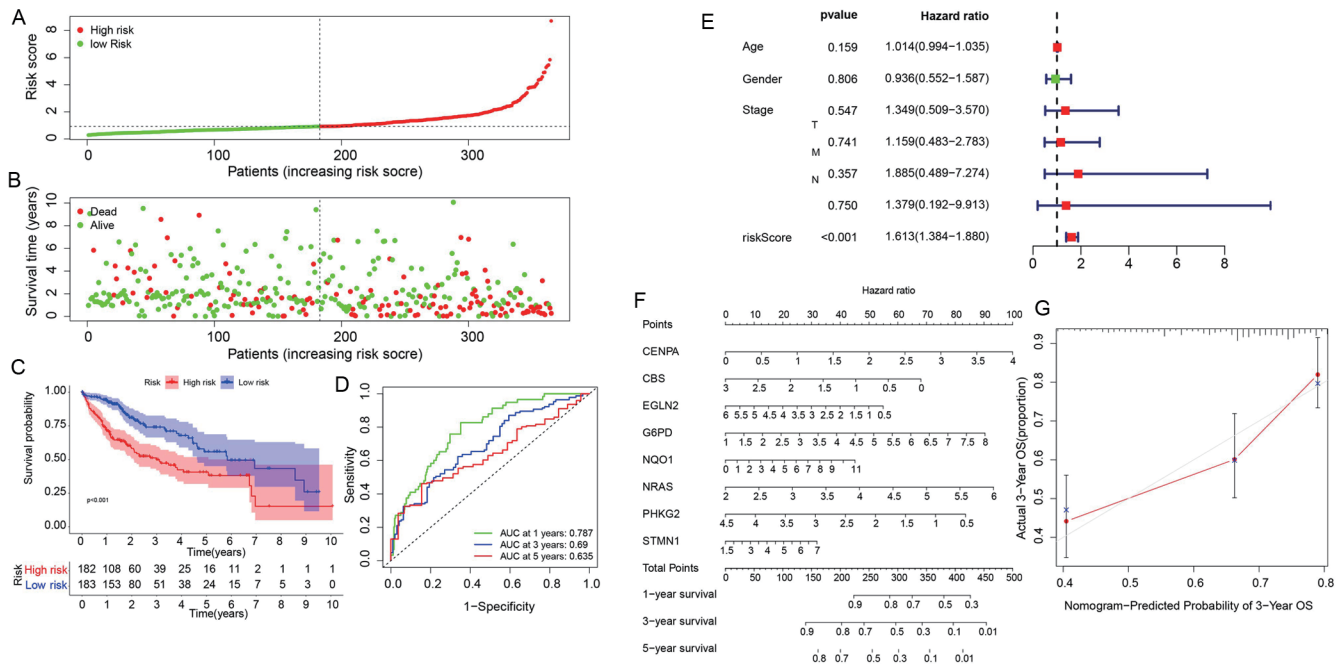
Fig. 4. Construction of a prognostic risk model for HCC patients. (A) HCC patients were assigned to high-risk and low-risk groups based on the multivariate Cox analysis results. Green indicates the low-risk group, and red indicates the high-risk group. The abscissa represents the distribution of risk values from low-risk to high-risk patients, and the ordinate represents the risk value. (B) The survival of HCC patients in the high-risk and low-risk groups. The abscissa represents the distribution of risk values from low-risk to high-risk patients, and the ordinate represents the survival time of patients. Green dots indicate the surviving patients, and red dots indicate dead patients. (C) Survival curves of HCC patients in the high-risk and low-risk groups. The abscissa shows survival time, and the ordinate shows the survival rate. Red lines indicate the high-risk group, and blue lines indicate the low-risk group. (D) Accuracy of the prognostic risk model in predicting the prognosis of HCC patients with the ROC curve. Green, blue, and red curves represent the ROC curve analysis of 1-, 3-, and 5-year survival, respectively. (E) Independent prognostic ability of the prognostic risk model. The left side indicates the risk values of each clinical trait and the prognostic model, and the middle shows *p*-value. *p*<0.05 suggests that the factor may be an independent prognostic factor. The hazard ratio (HR) represents the risk rate. Values >1 indicate high-risk genes and values <1 indicate low-risk genes. The right side shows the hazard ratio distribution of the gene. The distribution on the left side indicates low risk and the distribution on the right side represents high risk. (F) Construction of a nomogram based on eight prognosis-related genes. (G) Predictive power of the nomogram shown by the calibration curve. There are 182 patients in the high-risk group and 183 patients in the low-risk group. HCC, hepatocellular carcinoma.

group. Survival analysis (Fig. 4C) found that the OS rate of HCC patients was substantially lower in the high-risk group than in the low-risk group. As reflected by the results of ROC curve analysis (Fig. 4D), the AUC value of the prognostic risk model predicting 1–3 years of prognosis of HCC patients was >0.6. Moreover, multivariate Cox regression analysis (Fig. 4E) confirmed that the prognostic risk model served as an independent prognostic factor independent of other clinical traits. The gene nomogram was plotted based on the eight prognostic-related genes in the TF-ferrGene regulatory network (Fig. 4F, G), which could predict the 1-, 3-, and 5-year survival rates of patients according to the control nomogram of related gene expression in HCC patients. The above results indicated that the prognostic risk model constructed from the eight TF-ferrGene regulatory network-related genes accurately predicted the prognosis of HCC patients.

A prognostic risk model constructed based on the eight genes is tightly related to clinicopathological features of HCC patients

Further correlation analysis between the prognostic risk model and the clinicopathological characteristics of HCC patients in the TCGA dataset (Fig. 5) found that high-risk patients were significantly associated with the pathological stage and tumor spread of HCC patients, that is, high-risk patients had higher pathological stages, larger tumors, and more spreading. To sum up, the eight genes for constructing the prognostic risk model might exert pivotal regulatory

functions in the occurrence and development of HCC.

CENPA/STMN1 may be a key TF-ferrGene regulatory network involved in the ferroptosis of HCC

Next, this study further probed the key TF-ferrGene regulatory network involved in ferroptosis of HCC. We analyzed the expression of CENPA and STMN1 in collected HCC tissues (tumor group) and adjacent normal tissues (normal group) by RT-qPCR and western blot analysis. The results found that the expression of CENPA and STMN1 was significantly upregulated in HCC tissues (Fig. 6A). Moreover, AFP protein was only highly expressed in HCC cell lines Huh-7, JHH7, and SNU387 (Fig. 6B). The expression of genes related to the prognostic risk model for HCC was tested in Huh-7, JHH7, and SNU387 cells with RT-qPCR. It was found that CENPA and STMN1 were most upregulated in Huh-7, JHH7, and SNU387 cells as compared to THLE-2 cells (Fig. 6C), with the highest expression in Huh-7 cells. Subsequent experiments were conducted with Huh-7. According to the results of TF and ferrGene coexpression analysis (Fig. 6D), CENPA as a TF was positively correlated with the ferrGene STMN1. Therefore, it was speculated that CENPA elevated STMN1 transcription, promoted ferroptosis, and facilitated the growth of HCC.

To confirm the above speculation, CENPA was silenced or overexpressed in Huh-7 cells. RT-qPCR and western blot results (Fig. 6E, F) showed that mRNA and protein expression of CENPA and STMN1 was downregulated significantly
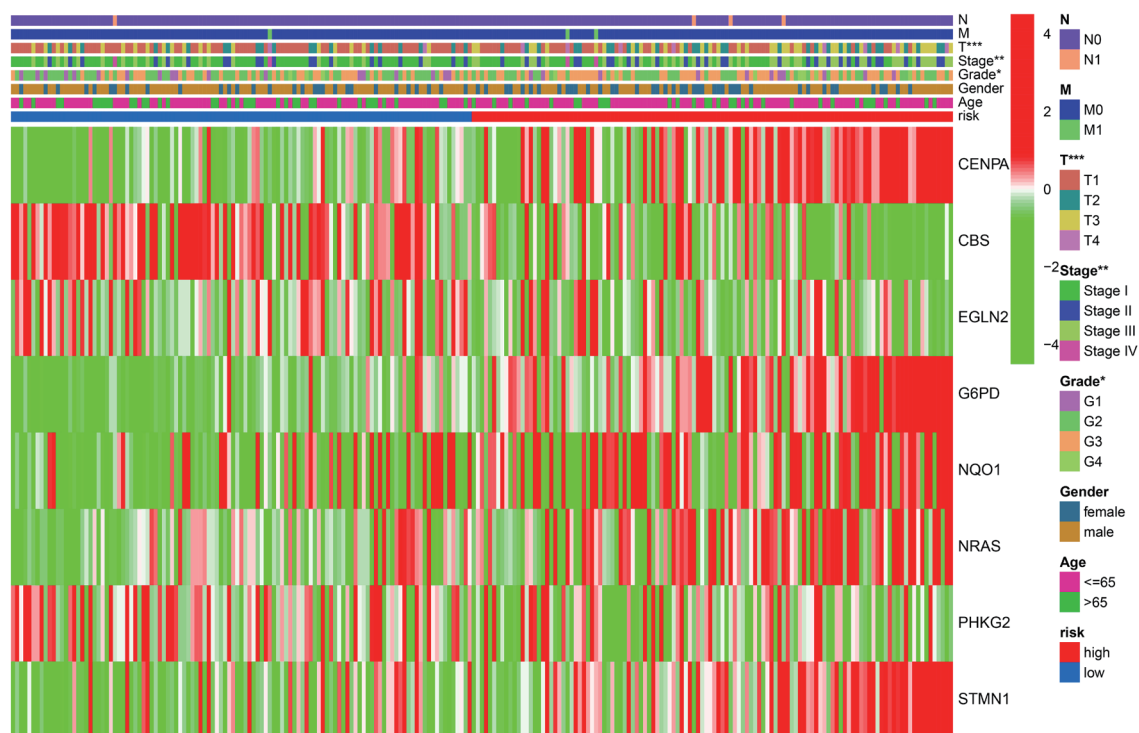
Fig. 5. Analysis of the correlation between the prognostic risk model and the clinical characteristics of HCC patients. A heatmap of the correlation between the prognostic risk model and the clinical characteristics of HCC patients is shown. The top right histogram is the color scale. Red indicates highly expressed genes, and green indicates poorly expressed genes. The upper panel shows each clinical trait and high and low prognostic risk values, respectively. The specific grouping of clinical traits is consistent with the labeling on the right, where the clinical traits correspond to *$p<0.05$, **$p<0.01$, and ***$p<0.001$. HCC, hepatocellular carcinoma.

after treatment with sh-CENPA, with the optimal silencing efficiency for the sh-CENPA-1 sequence. As a result, that sequence was selected for subsequent experiments. In addition, the mRNA and protein expression of CENPA and STMN1 was enhanced in response to oe-CENPA treatment. Moreover, the dual-luciferase assay (Fig. 6G) suggested that in the wild-type group, STMN1 promoter activity was significantly decreased after silencing CENPA and prominently increased after overexpressing CENPA. However, in the mutant group, neither silencing of CENPA nor overexpression of CENPA changed the STMN1 promoter activity. The ChIP assay results (Fig. 6H) demonstrated that CENPA enrichment at STMN1 promoter was diminished strikingly by CENPA silencing but augmented substantially by CENPA overexpression. These data illustrated that CENPA promoted STMN1 transcription by binding to the STMN1 promoter. Collectively, CENPA/STMN1 may be a key TF-ferrGene regulatory network participating in ferroptosis of HCC.

CENPA silencing facilitates HCC cell ferroptosis by restricting STMN1 transcription, thus curtailing HCC cell growth

Huh-7 cells were transfected with sh-NC + oe-NC, sh-CENPA + oe-NC, or sh-CENPA + oe-STMN1 to further clarify the effect of CENPA on HCC cell ferroptosis through regulating STMN1. As reflected by the RT-qPCR and western blot results (Fig. 7A), CENPA and STMN1 expression was decreased in Huh-7 cells treated with sh-CENPA. Furthermore, CENPA expression was unchanged and STMN1 expression was enhanced in Huh-7 cells after oe-STMN1 transfection in the presence of sh-CENPA.

For ELISA results (Fig. 7B, C), both GSH and GPX4 lev-

els were notably diminished and both MDA and ROS levels were prominently augmented in Huh-7 cells by CENPA silencing, which was reversed by further overexpressing STMN1. Meanwhile, Fe^{2+} content in Huh-7 cells was enhanced subsequent to CENPA silencing, which was abrogated by further overexpression of STMN1 (Fig. 7D). Flow cytometry (Fig. 7E) and CCK-8 (Fig. 7F) results documented that CENPA silencing resulted in an obvious elevation in the apoptosis and a substantial decline in the viability of Huh-7 cells, which was neutralized by further STMN1 overexpression. These results suggested that CENPA silencing augmented the ferroptosis of HCC cells by downregulating STMN1, thus curbing HCC cell growth.

Discussion

Currently, the available treatment options of HCC are limited with unsatisfactory clinical efficacy,[17] and molecular-targeted therapies have been clinically applied for the treatment of multiple cancers, like HCC.[18] Intriguingly, ferroptosis induction emerges as a therapeutic strategy against HCC.[19] On this basis, it is of significance to probe ferroptosis-related molecular mechanisms in HCC. Herein, the findings revealed that the TF CENPA might suppress HCC cell ferroptosis by promoting STMN1 transcription, thereby facilitating HCC cell growth.

As an extensively utilized and powerful research method for gene expression analysis, bioinformatics analysis simultaneously measures changes in the expression of numerous genes that have allowed identification of multiple DEGs implicated in HCC initiation and progression.[20] In previous studies, the ferrGenes have been analyzed with bioinformatics analysis in multiple cancers, including HCC.[21] In our study,
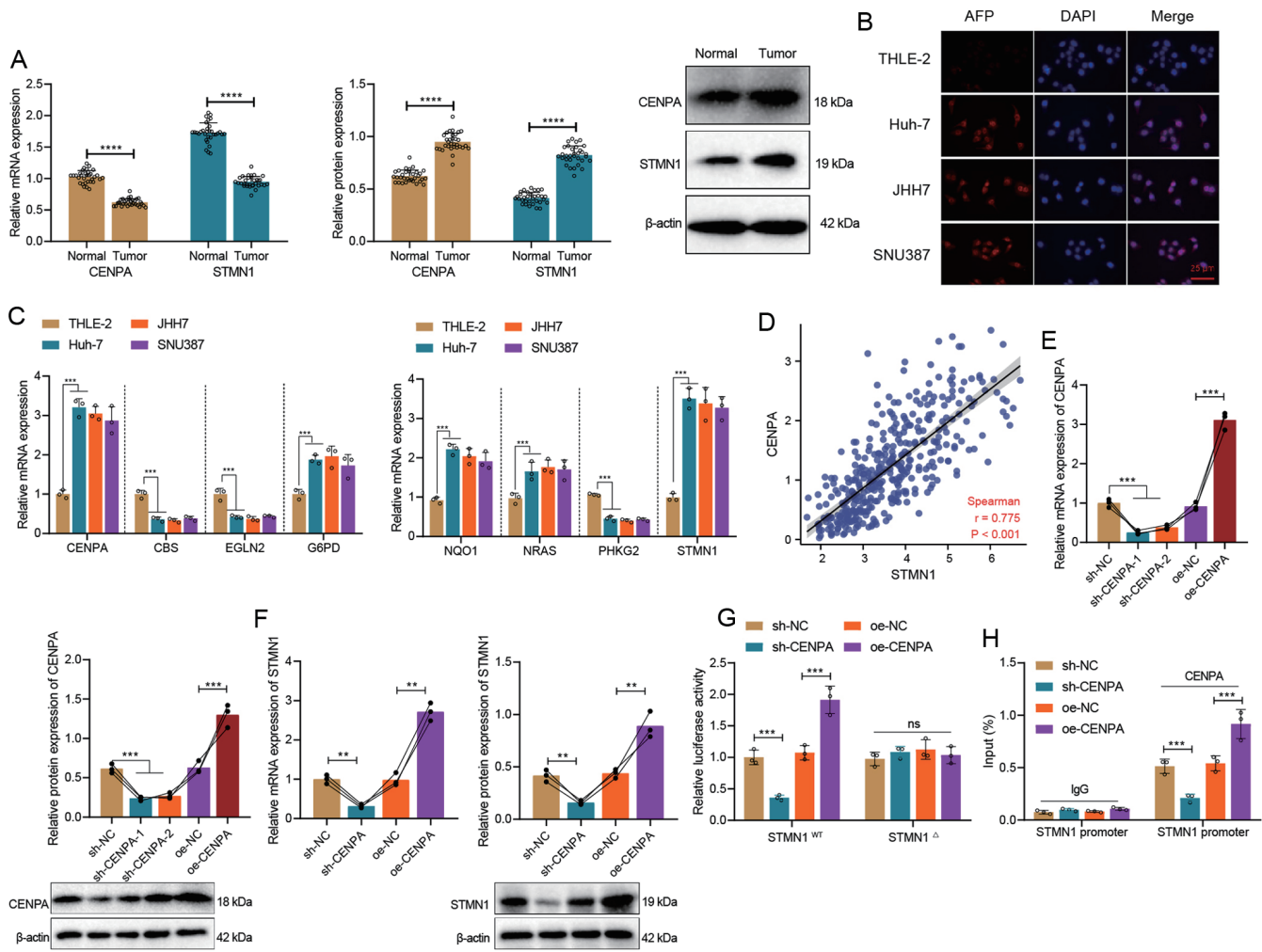
Fig. 6. Transcriptional regulation of STMN1 by CENPA. (A) Expression of CENPA and STMN1 in collected HCC tissues (tumor group) and adjacent normal tissues (normal group) determined by RT-qPCR and western blot analysis. (B) AFP expression in normal hepatocytes THLE-2 and HCC cell lines Huh-7, JHH7, and SNU387 determined by immunofluorescence. (C) Expression of genes involved in the prognostic risk model of HCC in normal hepatocytes THLE-2 as well as Huh-7, JHH7, and SNU387 HCC cells measured with RT-qPCR. (D) Spearman analysis of the correlation between CENPA and STMN1 expression in 374 HCC tissue samples. (E) CENPA mRNA and protein expression in Huh-7 cells determined in response to treatment with oe-CENPA or sh-CENPA determined by RT-qPCR. F, STMN1 mRNA and protein expression in Huh-7 cells measured in response to CENPA overexpression or silencing with RT-qPCR. (G) STMN1 promoter activity in wild-type and mutant groups tested with dual-luciferase assay. (H) CENPA enrichment at the STMN1 promoter assessed with the ChIP assay. *$p<0.05$, **$p<0.01$, and ***$p<0.001$. All cell experiments were repeated three times. HCC, hepatocellular carcinoma; CENPA, centromere protein A; STMN1, stathmin 1; oe-, overexpression; sh-, short hairpin RNA; ChIP, chromatin immunoprecipitation; RT-qPCR, reverse transcription-quantitative polymerase chain reaction.

we also used bioinformatics analysis, TCGA, and GTEx, to predict differentially expressed ferrGenes in HCC, yielding 24 upregulated genes and 21 downregulated genes. Moreover, the transcription of many genes is modulated by TFs.[22] Moreover, a previous study used the TCGA database to predict a TF-ferrGene regulatory network in liver cancer and found that ferrGenes were controlled by TFs, HIC1, and HNF4A.[23] Similarly, we used the TCGA database combined with GTEx database to retrieve 32 differentially expressed TFs in HCC. Then, these TFs and 45 differentially expressed ferrGenes were subjected to coexpression analysis to construct TF-ferrGene regulatory networks in HCC.

Subsequently, the clinical survival data of HCC patients in TCGA database were integrated with the gene expression data in the obtained TF-ferrGene regulatory networks. Eight genes closely related to the prognosis of HCC patients were obtained with Lasso regression and multivariate Cox analysis,

including high-risk (CENPA, G6PD, NQO1, NRAS, and STMN1) and low-risk (CBS, EGLN2, and PHKG2) genes, and were used to construct a prognostic risk model for HCC patients. Importantly, this prognostic risk model accurately predicted the prognosis of HCC patients and was tightly related to the clinicopathological characteristics of patients. Consistently, an earlier study elucidated that CENPA was a hazardous TF in HCC with a strong relation to the clinicopathological characteristics and prognoses of patients.[24] G6PD and NRAS, ferrGenes, were identified as a deleterious effectors linked to the prognosis of HCC.[25,26] Lin *et al*.[27] observed that NQO1 might be an independent biomarker for prognostic evaluation of HCC as its overexpression was associated with tumor size, venous infiltration, tumor-node-metastasis stage, and low disease-free survival, and 5-year survival rates. In addition, STMN1 is upregulated in HCC, which is linked to clinicopathological parameters and influences prognosis in HCC patients.[28] The
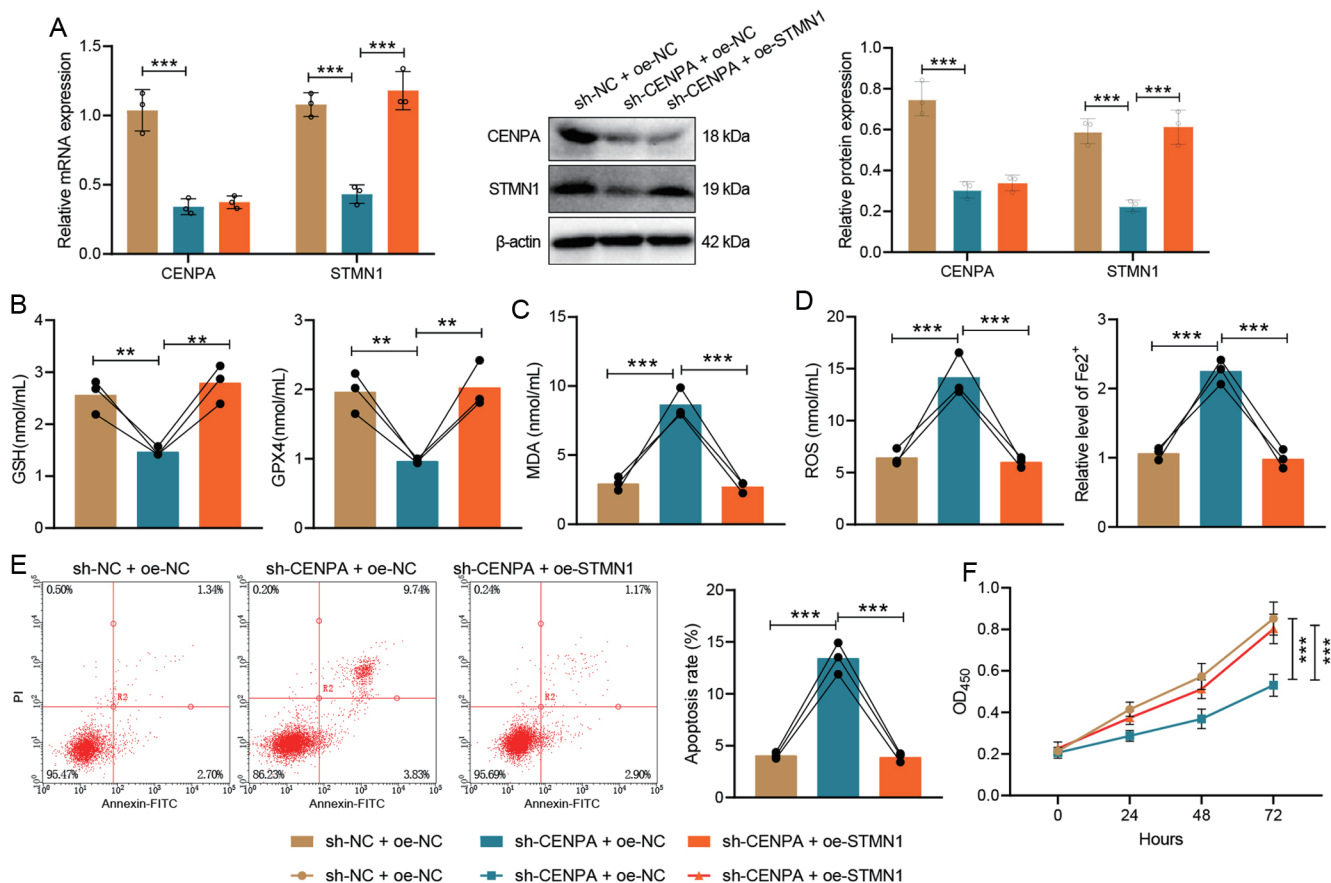
Fig. 7. CENPA silencing promotes ferroptosis and inhibits growth of HCC cells by downregulating STMN1. Huh-7 cells were transfected with sh-NC + oe-NC, sh-CENPA + oe-NC, and sh-CENPA + oe-STMN1. (A) CENPA and STMN1 expression in Huh-7 cells tested with RT-qPCR and western blot analysis. (B) ELISA to evaluate GSH and GPX4 expression. (C) ELISA to determine MDA and ROS levels in Huh-7 cells. (D) Fe^{2+} enrichment in Huh-7 cells measured with a kit. (E) Apoptosis of Huh-7 cells examined with flow cytometry. (F) CCK-8 to detect the viability of Huh-7 cells. $*p<0.05$, $**p<0.01$, and $***p<0.001$. all cell experiments were repeated three times. HCC, hepatocellular carcinoma; CENPA, centromere protein A; STMN1, stathmin 1; oe-, overexpression; sh-, short hairpin RNA; CCK-8, cell counting kit-8; ELISA, enzyme-linked immunosorbent assay; GPX4, glutathione peroxidase 4; GSH, glutathione; GTEx, Genotype-Tissue Expression; MDA, malondialdehyde; NC, negative control; ROS, reactive oxygen species; RT-qPCR, reverse transcription-quantitative polymerase chain reaction.

poor expression of CBS has been reported in HCC, which predicts the poor prognosis of HCC patients.[29] Likewise, the inactivation of the angiogenesis inhibitor EGLN2 is correlated with the poor prognosis of HCC.[30] Although the role of PHKG2 in HCC is rarely reported, it has been implicated in the prognosis of other cancers, such as lung adenocarcinoma.[31]

Moreover, our data shows that the CENPA/STMN1 axis may be a key TF-ferrGene regulatory network in HCC. Moreover, CENPA silencing augmented ferroptosis and apoptosis and depressed viability in HCC cells by downregulating STMN1, accompanied by downregulated GSH and GPX4 and upregulated MDA and ROS. Iron metabolism plays an important role in the process of ferroptosis, and accumulation of iron might induce ferroptosis.[32] A previous study has shown that the iron content is decreased in liver tumor tissues, accompanied by the changes in the expression of iron metabolism molecules; the silencing or overexpression of SLC46A1 can affect the intracellular iron content in HCC cells and tissues to control the iron homeostasis in HCC.[33] The accumulation of ROS, the consumption of GSH, the inhibition of GPX4 activity and the increase of MDA are considered to be the biological characteristics of ferroptosis.[32–35] System xc⁻/GSH/GPX4 is a potential molecular mechanism that induces ferroptosis in HCC.[36] Intriguingly, ROS, MDA and GSH can be used to

measure and evaluate the role and molecular mechanism of TEA domain transcription factor 1 (TEAD1) in HCC and its effect on sorafenib-induced ferroptosis.[37] Therefore, assays of ROS, MDA, GSH, and GPX4 comprehensively evaluate the occurrence of ferroptosis in HCC cells.

As reported, CENPA functions as an oncogenic and is overexpressed in numerous cancers, including clear cell renal cell carcinoma, ovarian cancer, and breast cancer.[38–40] Furthermore, CENPA is abundantly expressed in HCC tissues and CENPA silencing diminishes proliferation and enhances apoptosis in HCC cells.[41] In addition, a former study unveiled the implication of CENPA downregulation in Sig-1R deficiency-caused elevations in ROS levels in beta cells, partially concurrent with our result.[42] Importantly, CENPA has been confirmed as a transcription activator.[43] Intriguingly, both STMN1 and CENPA has been observed to be upregulated in HCC.[44] Therefore, CENPA might transcriptionally activate STMN1 to induce the development of HCC. Of note, our dual-luciferase and ChIP assays demonstrated that CENPA bound to STMN1 promoter to induce STMN1 transcription. Further rescue experiments unraveled that overexpression of STMN1 nullified the effects of CENPA silencing on the growth and ferroptosis of HCC cells. It should be noted that the role of CENPA in ferroptosis has been rarely reported. However, STMN1 has
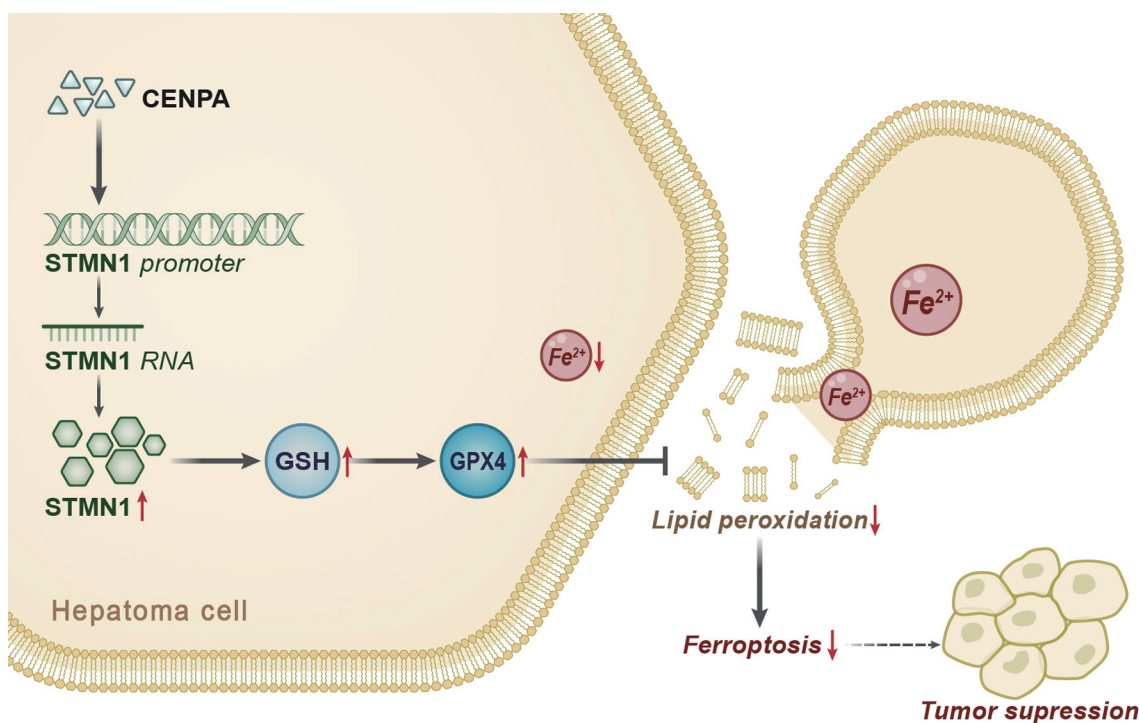
Fig. 8. Schematic illustration of the molecular mechanisms. CENPA suppresses ferroptosis and promotes growth of HCC cells by upregulating the STMN1 transcription. HCC, hepatocellular carcinoma; CENPA, centromere protein A; STMN1, stathmin 1.

been reported to as an important ferrGene in coronary artery disease,[45] soft tissue sarcoma,[46] adrenocortical carcinoma.[47] Similarly, the research of Wang *et al*.[48] exhibited that STMN1 was a ferrGene that correlated to the poor survival of HCC. Moreover, STMN1 was identified as a prognostically relevant methylation-driven ferrGene in HCC, with diminished methylation level of STMN1 found in HCC tissues.[49] Nevertheless, the specific regulatory mechanism of STMN1 in ferroptosis still remains elusive.

In conclusion, our findings elucidated that CENPA attenuated the ferroptosis of HCC cells by transcriptionally activating STMN1, thus inducing HCC cell growth (Fig. 8). This study provides novel mechanistic understanding and molecular targets for the treatment of HCC. However, the data for the construction of the present prognostic risk model were obtained from public databases. Transcriptome sequencing may obtain more representative results if they are available for analysis in subsequent studies. Moreover, *in vivo* experiments are needed to further substantiate the findings.

Conflict of interest

The authors have no conflict of interests related to this publication.

Author contributions

Writing of the paper and conception and design of the experiments **(**DL, LL, JW), analysis of the data (TL, CG), and collection and provision of the sample for this study (DL, LL). All authors have read and approved the final submitted manuscript.

Ethical statement

The study was approved by the Ethics Committee of our Hospital and conducted in strict accordance with the Declaration of Helsinki. All participants signed informed consent documentation before sample collection.

Data sharing statement

The data that supports the findings of this study are available on request from the corresponding author.

References

[1] El-Serag HB. Epidemiology of viral hepatitis and hepatocellular carcinoma. Gastroenterology 2012;142(6):1264–1273.e1. doi:10.1053/j.gastro.2011.12.061, PMID:22537432.
[2] Kulik L, El-Serag HB. Epidemiology and Management of Hepatocellular Carcinoma. Gastroenterology 2019;156(2):477–491.e1. doi:10.1053/j.gastro.2018.08.065, PMID:30367835.
[3] Chidambaranathan-Reghupaty S, Fisher PB, Sarkar D. Hepatocellular carcinoma (HCC): Epidemiology, etiology and molecular classification. Adv Cancer Res 2021;149:1–61. doi:10.1016/bs.acr.2020.10.001, PMID:33579421.
[4] Capelletti MM, Manceau H, Puy H, Peoc'h K. Ferroptosis in Liver Diseases: An Overview. Int J Mol Sci 2020;21(14):4908. doi:10.3390/ijms21144908, PMID:32664576.
[5] Ursini F, Maiorino M. Lipid peroxidation and ferroptosis: The role of GSH and GPx4. Free Radic Biol Med 2020;152:175–185. doi:10.1016/j.freeradbiomed.2020.02.027, PMID:32165281.
[6] Gan B. Mitochondrial regulation of ferroptosis. J Cell Biol 2021;220(9): e202105043. doi:10.1083/jcb.202105043, PMID:34328510.
[7] Bekric D, Ocker M, Mayr C, Stintzing S, Ritter M, Kiesslich T, *et al*. Ferroptosis in Hepatocellular Carcinoma: Mechanisms, Drug Targets and Approaches to Clinical Translation. Cancers (Basel) 2022;14(7):1826. doi:10.3390/cancers14071826, PMID:35406596.

[8] Liang JY, Wang DS, Lin HC, Chen XX, Yang H, Zheng Y, *et al*. A Novel Ferroptosis-related Gene Signature for Overall Survival Prediction in Patients with Hepatocellular Carcinoma. Int J Biol Sci 2020;16(13):2430–2441. doi:10.7150/ijbs.45050, PMID:32760210.

[9] Yang M, Wu X, Hu J, Wang Y, Wang Y, Zhang L, *et al*. COMMD10 inhibits HIF1α/CP loop to enhance ferroptosis and radiosensibility by disrupting Cu-Fe balance in hepatocellular carcinoma. J Hepatol 2022;76(5):1138–1150. doi:10.1016/j.jhep.2022.01.009, PMID:35101526.

[10] Chen A, Koehler AN. Transcription Factor Inhibition: Lessons Learned and Emerging Targets. Trends Mol Med 2020;26(5):508–518. doi:10.1016/j.molmed.2020.01.004, PMID:32359481.

[11] Bushweller JH. Targeting transcription factors in cancer - from undruggable to reality. Nat Rev Cancer 2019;19(11):611–624. doi:10.1038/s41568-019-0196-7, PMID:31511663.

[12] Song J, Xie C, Jiang L, Wu G, Zhu J, Zhang S, *et al*. Transcription factor AP-4 promotes tumorigenic capability and activates the Wnt/β-catenin pathway in hepatocellular carcinoma. Theranostics 2018;8(13):3571–3583. doi:10.7150/thno.25194, PMID:30026867.

[13] Chen RX, Xia YH, Xue TC, Ye SL. Transcription factor c-Myb promotes the invasion of hepatocellular carcinoma cells via increasing osteopontin expression. J Exp Clin Cancer Res 2010;29(1):172. doi:10.1186/1756-9966-29-172, PMID:21190594.

[14] Pan Y, Tsai CJ, Ma B, Nussinov R. Mechanisms of transcription factor selectivity. Trends Genet 2010;26(2):75–83. doi:10.1016/j.tig.2009.12.003, PMID:20074831.

[15] Nishizawa H, Matsumoto M, Shindo T, Saigusa D, Kato H, Suzuki K, *et al*. Ferroptosis is controlled by the coordinated transcriptional regulation of glutathione and labile iron metabolism by the transcription factor BACH1. J Biol Chem 2020;295(1):69–82. doi:10.1074/jbc.RA119.009548, PMID:31740582.

[16] Luk ST, Ng KY, Zhou L, Tong M, Wong TL, Yu H, *et al*. Deficiency in Embryonic Stem Cell Marker Reduced Expression 1 Activates Mitogen-Activated Protein Kinase Kinase 6-Dependent p38 Mitogen-Activated Protein Kinase Signaling to Drive Hepatocarcinogenesis. Hepatology 2020;72(1):183–197. doi:10.1002/hep.31020, PMID:31680287.

[17] Tu T, Budzinska MA, Maczurek AE, Cheng R, Di Bartolomeo A, Warner FJ, *et al*. Novel aspects of the liver microenvironment in hepatocellular carcinoma pathogenesis and development. Int J Mol Sci 2014;15(6):9422–9458. doi:10.3390/ijms15069422, PMID:24871369.

[18] Alqahtani A, Khan Z, Alloghbi A, Said Ahmed TS, Ashraf M, Hammouda DM. Hepatocellular Carcinoma: Molecular Mechanisms and Targeted Therapies. Medicina (Kaunas) 2019;55(9):526. doi:10.3390/medicina55090526, PMID:31450841.

[19] Ajoolabady A, Tang D, Kroemer G, Ren J. Ferroptosis in hepatocellular carcinoma: mechanisms and targeted therapy. Br J Cancer 2023;128(2):190–205. doi:10.1038/s41416-022-01998-x, PMID:36229582.

[20] Zhang C, Peng L, Zhang Y, Liu Z, Li W, Chen S, *et al*. The identification of key genes and pathways in hepatocellular carcinoma by bioinformatics analysis of high-throughput data. Med Oncol 2017;34(6):101. doi:10.1007/s12032-017-0963-9, PMID:28432618.

[21] Xu Z, Peng B, Liang Q, Chen X, Cai Y, Zeng S, *et al*. Construction of a Ferroptosis-Related Nine-lncRNA Signature for Predicting Prognosis and Immune Response in Hepatocellular Carcinoma. Front Immunol 2021;12:719175. doi:10.3389/fimmu.2021.719175, PMID:34603293.

[22] Schleif RF. Modulation of DNA binding by gene-specific transcription factors. Biochemistry 2013;52(39):6755–6765. doi:10.1021/bi400968e, PMID:23962133.

[23] Introini-Collison IB, McGaugh JL. Naloxone and beta-endorphin alter the effects of post-training epinephrine on memory. Psychopharmacology (Berl) 1987;92(2):229–235. doi:10.1007/BF00177921, PMID:3110846.

[24] Xu R, Lin L, Zhang B, Wang J, Zhao F, Liu X, *et al*. Identification of prognostic markers for hepatocellular carcinoma based on the epithelial-mesenchymal transition-related gene BIRC5. BMC Cancer 2021;21(1):687. doi:10.1186/s12885-021-08390-7, PMID:34112092.

[25] Yuan C, Yuan M, Chen M, Ouyang J, Tan W, Dai F, *et al*. Prognostic Implication of a Novel Metabolism-Related Gene Signature in Hepatocellular Carcinoma. Front Oncol 2021;11:666199. doi:10.3389/fonc.2021.666199, PMID:34150630.

[26] Du X, Zhang Y. Integrated Analysis of Immunity- and Ferroptosis-Related Biomarker Signatures to Improve the Prognosis Prediction of Hepatocellular Carcinoma. Front Genet 2020;11:614888. doi:10.3389/fgene.2020.614888, PMID:33391356.

[27] Lin L, Sun J, Tan Y, Li Z, Kong F, Shen Y, *et al*. Prognostic implication of NQO1 overexpression in hepatocellular carcinoma. Hum Pathol 2017;69:31–37. doi:10.1016/j.humpath.2017.09.002, PMID:28964792.

[28] Zhang ED, Li C, Fang Y, Li N, Xiao Z, Chen C, *et al*. STMN1 as a novel prognostic biomarker in HCC correlating with immune infiltrates and methylation. World J Surg Oncol 2022;20(1):301. doi:10.1186/s12957-022-02768-y, PMID:36127700.

[29] Zhou YF, Song SS, Tian MX, Tang Z, Wang H, Fang Y, *et al*. Cystathionine β-synthase mediated PRRX2/IL-6/STAT3 inactivation suppresses Tregs infiltration and induces apoptosis to inhibit HCC carcinogenesis. J Immunother Cancer 2021;9(8):e003031. doi:10.1136/jitc-2021-003031, PMID:34413167.

[30] Calvisi DF, Ladu S, Gorden A, Farina M, Lee JS, Conner EA, *et al*. Mechanistic and prognostic significance of aberrant methylation in the molecular pathogenesis of human hepatocellular carcinoma. J Clin Invest 2007;117(9):2713–2722. doi:10.1172/JCI31457, PMID:17717605.

[31] Ren Z, Hu M, Wang Z, Ge J, Zhou X, Zhang G, *et al*. Ferroptosis-Related Genes in Lung Adenocarcinoma: Prognostic Signature and Immune, Drug Resistance, Mutation Analysis. Front Genet 2021;12:672904. doi:10.3389/fgene.2021.672904, PMID:34434214.

[32] Stockwell BR, Friedmann Angeli JP, Bayir H, Bush AI, Conrad M, Dixon SJ, *et al*. Ferroptosis: A Regulated Cell Death Nexus Linking Metabolism, Redox Biology, and Disease. Cell 2017;171(2):273–285. doi:10.1016/j.cell.2017.09.021, PMID:28985560.

[33] Wang D, Wu H, Yang J, Li M, Ling C, Gao Z, *et al*. Loss of SLC46A1 decreases tumor iron content in hepatocellular carcinoma. Hepatol Commun 2022;6(10):2914–2924. doi:10.1002/hep4.2031, PMID:35811443.

[34] Wu J, Wang Y, Jiang R, Xue X, Yin X, Wu M, *et al*. Ferroptosis in liver disease: new insights into disease mechanisms. Cell Death Discov 2021;7(1):276. doi:10.1038/s41420-021-00660-4, PMID:34611144.

[35] Dixon SJ, Lemberg KM, Lamprecht MR, Skouta R, Zaitsev EM, Gleason CE, *et al*. Ferroptosis: an iron-dependent form of nonapoptotic cell death. Cell 2012;149(5):1060–1072. doi:10.1016/j.cell.2012.03.042, PMID:22632970.

[36] Li L, Wang X, Xu H, Liu X, Xu K. Perspectives and mechanisms for targeting ferroptosis in the treatment of hepatocellular carcinoma. Front Mol Biosci 2022;9:947208. doi:10.3389/fmolb.2022.947208, PMID:36052168.

[37] Li H, Lan H, Zhang M, Zhao F, An N, Yi C. TEA Domain Transcription Factor 1 Inhibits Ferroptosis and Sorafenib Sensitivity of Hepatocellular Carcinoma Cells. Dig Dis Sci 2023. doi:10.1007/s10620-023-07824-5, PMID: 36680063.

[38] Wang Q, Xu J, Xiong Z, Xu T, Liu J, Liu Y, *et al*. CENPA promotes clear cell renal cell carcinoma progression and metastasis via Wnt/β-catenin signaling pathway. J Transl Med 2021;19(1):417. doi:10.1186/s12967-021-03087-8, PMID:34627268.

[39] Han J, Xie R, Yang Y, Chen D, Liu L, Wu J, *et al*. CENPA is one of the potential key genes associated with the proliferation and prognosis of ovarian cancer based on integrated bioinformatics analysis and regulated by MYBL2. Transl Cancer Res 2021;10(9):4076–4086. doi:10.21037/tcr-21-175, PMID:35116705.

[40] Ding Y, Li Y, Duan Y, Wang W, Zheng W, Cheng W, *et al*. LncRNA MBNL1-AS1 Represses Proliferation and Cancer Stem-Like Properties of Breast Cancer through MBNL1-AS1/ZFP36/CENPA Axis. J Oncol 2022;2022:9999343. doi:10.1155/2022/9999343, PMID:35518784.

[41] Li Y, Zhu Z, Zhang S, Yu D, Yu H, Liu L, *et al*. ShRNA-targeted centromere protein A inhibits hepatocellular carcinoma growth. PLoS One 2011;6(3):e17794. doi:10.1371/journal.pone.0017794, PMID:21423629.

[42] Ke M, He G, Wang H, Cheng S, Xu Y. Sigma receptor knockdown augments dysfunction and apoptosis of beta cells induced by palmitate. Exp Biol Med (Maywood) 2021;246(13):1491–1499. doi:10.1177/1535370221997780, PMID:33715527.

[43] Liang YC, Su Q, Liu YJ, Xiao H, Yin HZ. Centromere Protein A (CENPA) Regulates Metabolic Reprogramming in the Colon Cancer Cells by Transcriptionally Activating Karyopherin Subunit Alpha 2 (KPNA2). Am J Pathol 2021;191(12):2117–2132. doi:10.1016/j.ajpath.2021.08.010, PMID:345 08688.

[44] Jiang L, Zhao L, Bi J, Guan Q, Qi A, Wei Q, *et al*. Glycolysis gene expression profilings screen for prognostic risk signature of hepatocellular carcinoma. Aging (Albany NY) 2019;11(23):10861–10882. doi:10.18632/aging.102489, PMID:31790363.

[45] Wu X, Qin K, Iroegbu CD, Xiang K, Peng J, Guo J, *et al*. Genetic analysis of potential biomarkers and therapeutic targets in ferroptosis from coronary artery disease. J Cell Mol Med 2022;26(8):2177–2190. doi:10.1111/jcmm.17239, PMID:35152560.

[46] Zhao J, Zhao Y, Ma X, Feng H, Cui R. Immunological and prognostic significance of novel ferroptosis-related genes in soft tissue sarcoma. PLoS One 2022;17(1):e0262234. doi:10.1371/journal.pone.0262234, PMID:34982796.

[47] Lin C, Hu R, Sun F, Liang W. Ferroptosis-based molecular prognostic model for adrenocortical carcinoma based on least absolute shrinkage and selection operator regression. J Clin Lab Anal 2022;36(6):e24465. doi:10.1002/jcla.24465, PMID:35500219.

[48] Wang H, Yang C, Jiang Y, Hu H, Fang J, Yang F. A novel ferroptosis-related gene signature for clinically predicting recurrence after hepatectomy of hepatocellular carcinoma patients. Am J Cancer Res 2022;12(5):1995–2011. PMID:35693077.

[49] Zhang Y, Ren H, Zhang C, Li H, Guo Q, Xu H, *et al*. Development and validation of four ferroptosis-related gene signatures and their correlations with immune implication in hepatocellular carcinoma. Front Immunol 2022;13:1028054. doi:10.3389/fimmu.2022.1028054, PMID:36304446.